

Original Article

Adsorption and inhibition analysis of aconitine and tubocurarine alkaloids as eco-friendly inhibitors of pitting corrosion in ASTM – A47 low carbon steel in HCl acid environment

Benedict Ushaka Ugi^{1*}, Victoria Mfon Bassey¹, Mbang Eze Obeten²,
Stephen Adie Adalikwu³, Chijioke Everistus Omaliko¹, and Desmond Obi Nandi¹

¹ *Department of Pure and Applied Chemistry, Faculty of Physical Science,
University of Calabar, Calabar, Nigeria*

² *Department of Chemistry, Faculty of Science,
University of Cross River State, Calabar, Nigeria*

³ *Department of Chemistry, Faculty of Science,
College of Education Akamkpa, Akamkpa, Nigeria*

Received: 22 June 2021; Revised: 24 September 2021; Accepted: 23 November 2021

Abstract

The research on the adsorption and inhibition analysis of aconitine alkaloid (ACA) and tubocurarine alkaloid (TBA) as eco-friendly inhibitors of pitting corrosion in ASTM – A47 low carbon steel in HCl acid was carried out under the following experimental and analytical methods: gravimetric method, electrochemical impedance spectroscopy, potentiodynamic polarization, and scanning electron microscopy method. Results revealed good inhibitors as inhibition efficiencies were recorded at 98.8% and 91.2% for tubocurarine and aconitine alkaloids, respectively. Electrochemical data strongly supported the efficacy of both inhibitors as earlier presented by the chemical methods as trend in values of charge transfer resistance, double layer capacitance, etc. Were in accordance with standards for a good inhibitor. The inhibitors were seen to be spontaneous, stabled, endothermic and physically adsorbed. Adsorption of the inhibitors on metal surface obeyed Langmuir, El-Awady, Freundlich, and Temkin adsorption isotherm. A monolayer physical adsorption was defined for the system.

Keywords: tubocurarine, aconitine, alkaloids, corrosion, polarization, adsorption, impedance

1. Introduction

Corrosion generally is a serious social and economic disadvantage such that millions of dollars have been already spent by different countries in combatting its menace. On a normal day, corrosion can be defined from the instance of deterioration of a material, especially metal, when exposed to an aggressive environment, possible to cause anodic metal dissolution or cathodic hydrogen evolution (Bardal, 2004; Davis, 2000; Gergely, 2019). Disadvantages of corrosion

irrespective of types have been long discovered in many areas ranging from leakages of oil crude at truck pipelines, leakages of food from cans, failure of bridges at different intervals, etc. (Davis, 2000; Gergely, 2019; McCafferty, 2010; Ohtsuka, Nishikata, Sakari, & Fushimi, 2018). Pitting corrosion is a localized form of corrosion that involves the formation of cavities and holes in a material (Bardal, 2004; Davis, 2000; Ohtsuka *et al.*, 2018 ; Perez, 2016). For a defect-free perfect material, pitting corrosion could arise from the environment as a factor that may contain aggressive chemical species damaging to the passive film (oxide) hence initiate pitting at oxide breaks (Bardal, 2004; McCafferty, 2010; Rajendran, Nguyen, Kakoei, Li, & Yeganeh, 2020).

*Corresponding author

Email address: ugibenedit@gmail.com

The interest in corrosion inhibitors came from their ready availability, non-toxic and eco-friendly nature, and cost-effectiveness, among others (Baddal, 2004; Davis, 2000; Talbot & Talbot, 2018). Very interestingly, their ability to adsorb on the metal surface forming protective films, strong ability to combine with corrosion product films to protect the metal surface and formation of precipitates which visibly coat and protect metal surfaces consequence upon the possession of hetero-compounds and atoms, double bonds, benzene rings, and pie-bond led to usage in testing corrosion inhibition of ASTM – A47 low carbon steel in HCl acid environment (Gergely, 2019; McCafferty, 2010; Talbot & Talbot, 2018).

In line with growing research in the field of organic and eco-friendly corrosion inhibitors as control measures of metal anodic dissolution and cathodic hydrogen evolution, this research in corrosion science and electrochemistry was carried out in order to investigate the adsorption and inhibition analysis of aconitine alkaloid and tubocurarine alkaloid as eco-friendly inhibitors of pitting corrosion in ASTM – A47 Low Carbon Steel in HCl acid.

2. Materials and Methods

The materials used for this research are as follows: *Chondrodendron tomentosum* and *Aconitum napellus* plants, ethanol, diethyl ether, hydrochloric acid, ammonia, hydrobromic acid, tubocurarine alkaloid, tartaric acid, 1000 mL volumetric flask, electronic UNIPOL-820 metallographic polishing machine, ADAM PGW 253e electronic digital weighing balance, distilled water, emery paper, acetone. In the course of this research, the following instrumentations used were M36 MEMERY Oven, separating funnel of 500 mL, Soxhlet extraction (heat extraction) process, gravimetric method, gasometric method, electrochemical impedance spectroscopy, potentiodynamic polarization, and scanning electron microscopy.

2.1 Preparation of stock solution, inhibitors, and metal dressing

The bark of *Chondrodendron tomentosum* and the roots of *Aconitum napellus* plants were both obtained from the bush around the boundary between the Obudu local government area of Cross River State and Tsa Local government area of Benue State, Nigeria. Both plant parts were brought to the Ultra-modern Petroleum Trust Fund Laboratory at the University of Calabar – Nigeria, where they were washed thoroughly to remove sand and other external materials and dried in an M36 MEMERY Oven at 55 °C for 48 h. The dried parts were removed, ground to a powdered form, and sieved to attain a smaller surface area for better surface coverage and optimal extraction. Extraction of 200 g powdered form of the roots and stem separately was carried out using a Soxhlet extractor (heat extraction) for 72 h in ethanol as solvent. The crude ethanol extracts were then evaporated in a water bath for 3.5 h each to concentrate the crude through the removal of retained ethanol to at least one-tenth of the original concentration. In order to isolate each of the alkaloids from the crude extract, a separating funnel of 500 mL was used. Two hundred mL of 0.5 M HCl was measured into the separating funnel containing 50 g of the crude extract. This was followed immediately by 200 mL

diethyl ether to wash and remove resins and fatty materials. The mixture was separated from the non-alkaloids contents while the diethyl ether content was made alkaline (to reduce the acidic content) with excess ammonia and another 150 mL diethyl ether plus 200 mL dilute hydrobromic acid solution to isolate the aconitine alkaloid. For the isolation of tubocurarine alkaloid, tartaric acid was used in place of hydrobromic acid, and the sample was collected in semi-solid form. Seven grams of each alkaloid was weighed into a 1000 mL volumetric flask and digested with 1 M HCl solution, allowed for 24 h for proper absorption and dissolution, then filtered and stored as inhibitors.

2.2 Gravimetric method

Gravimetric, or as it is called, weight loss analysis, was carried out on a 5.0 × 1.5 cm diameter low carbon steel every 24 h for 168 h. The resized metals earlier polished mechanically to mirror surface were weighed using ADAM PGW 253e electronic digital weighing balance. They were then immersed into 100 mL beakers containing different concentrations of each inhibitor (300, 500, 750, 1000, 1250, and 1500 ppm) by suspension and allowed for 24 h. After every 24 h, the metals were removed, washed with distilled water, degreased in ethanol, rinsed in acetone, and air-dried, then reweighed to obtain the different loss in weight of metals. The experiment was duplicated and mean taken to allow for accuracy. All reagents were of analar grade. The corrosion rate of the low carbon steel in both the presence and absence of inhibitors was determined from the slope of the plot of weight loss against time; the surface coverage and inhibition efficiency were obtained from Equation (1) and (2), respectively.

$$\theta = \frac{Wl_b - Wl_i}{Wl_b} \quad (1)$$

$$IE\% = \frac{Wl_b - Wl_i}{Wl_b} \times 100 \quad (2)$$

where θ is the surface coverage, Wl_b and Wl_i are the weight loss of blank and inhibitor respectively, $IE\%$ is the percentage inhibitor efficiency.

2.3 Electrochemical impedance method

The EIS was investigated at ambient temperature in a triple electrode cell compartment using Gamry Reference 600 potentiostat inclusive of a Gamry framework EIS300 system. Echem analyst software was used to analyze the fitting of the data. A saturated calomel (SCE) electrode was introduced as the reference electrode, and a 1 cm² platinum foil was introduced as a counter electrode. The working electrode with dimension 1 cm × 1 cm was dipped in 1 M HCl acid. Electrochemical tests were conducted within a frequency of 10–10,000 Hz within potentiodynamic conditions, with an amplitude of 5 mV, involving alternating current signals at E_{corr} . All experiments were conducted every 60 min with and without various concentrations of the inhibitors. From the R_{ct} obtained, the retardation efficiency was calculated using Equation (3):

$$IE\% = \frac{R_{ct}^i - R_{ct}^0}{R_{ct}^i} \times 100 \quad (3)$$

where R_{ct}^0 and R_{ct}^i represent the charge transfer resistance with and without the inhibitors.

2.4 Potentiodynamic polarization method

The potentiodynamic polarization curves were measured at a scan rate of 1 mV s^{-1} , from -500 to 0 mV versus SCE. The Tafel curves for the anode and cathode for low carbon steel dissolution were recorded in both the presence and absence of the inhibitor. Extrapolation of the linear segments of the anodic and cathodic curves gives useful parameters, including anodic and cathodic Tafel slopes, corrosion potential (E_{corr}), and corrosion current density (i_{corr}). The corrosion current density (i_{corr}) was used to calculate the inhibition efficiency of the inhibitors given by Equation (4):

$$\%IE_{pdp} = \left(1 - \frac{I_{corr}}{I_{corr}^0} \right) \times 100 \quad (4)$$

2.5 Scanning electron microscope analysis

The Scanning electron microscopic study was conducted using the JSM-5600 LV instrument (Hitachi) at the accelerating voltage of 15 kV . For the SEM study, the ASTM – A47 low carbon steel resized metals were allowed to corrode in 1 M HCl solution in the presence and absence of the inhibitors (1 M HCl , 300 ppm , and 1500 ppm); after that, the surfaces of the coupons were examined for their morphological changes.

3. Results and Discussion

3.1 Gravimetric analysis / Results

Gravimetric experiment explains the extent of molecular adsorption or desorption in a metal subjected to strong acid condition with or without inhibitor (corrosion) with respect to immersion time and concentration. According to this method, the higher the inhibition efficiency, the higher the inhibitor molecular adsorption on metal surface and

reduced weight loss of metal (corrosion rate drop) by acid attack. Research findings from the gravimetric experimentation in Table 1 showed increasing inhibition efficiency for both alkaloids (aconitine and tubocurarine) as concentration was increased up to 1500 ppm . This observation could generally be attributed to the strong binding power (molecular adsorption), large surface area coverage of both inhibitors on the low carbon steel surface (Al-Shehri, 2019; Faiza, Zahari, Awang, & Hussin, 2020; Go *et al.*, 2020; Lavanya, Priya, & Vijaya, 2020). This effect has a contrary impact on the corrosion rate of the metal in various concentrations as corrosion rate values were found to be decreasing from 0.934 in 1 M HCl solutions to 0.083 and 0.011 ppm for aconitine and tubocurarine alkaloids, respectively, as earlier observed in a similar work by Al-Shehri (2019), Bharatiya, Gal, Agrawal, Shah, and Sircar, (2019). Comparing inhibition efficiencies of both aconitine and tubocurarine alkaloids, it was observed that low carbon steel was less inhibited in aconitine alkaloids (91.2%) compared to tubocurarine alkaloids (98.8%). This could be due to the presence of more hetero-atoms (2N), pi bonds from double bonds, and benzene rings, including proper orientation of the molecular structure on metal during adsorption (Lavanya *et al.*, 2020; Majd, Ramezanzadeh, Ramezanzadeh, & Bahlakeh, 2020).

3.2 Electrochemical impedance spectroscopy

The electrochemical methods allow us to determine the relationship between the ionic, molecular, or charge transfer between the inhibitors and the metal surface in a conducting medium. In this experimental procedure, important information relating to the metal/inhibitor interaction like charge transfer resistance, double layer capacitance, surface coverage, and inhibition efficiency are unraveled. However, data for the double-layer capacitance for the semicircles and inhibition efficiency were calculated using Equation (5) and (6)

$$C_{dl} = \frac{1}{\omega Z''} \quad (5)$$

where Z'' is imaginary component of impedance at any frequency inside the semicircle and ω is the angular frequency. But $\omega = 2 * \pi * f_{max}$ (in Hz used for measurement of EIS).

Table 1. Gravimetric analysis data revealing corrosion rate of metal, surface coverage, and inhibition efficiency of inhibitors on ASTM – A47 low carbon steel in 1 M HCl

Inhibitor Conc. (ppm)	Aconitine alkaloid			Tubocurarine alkaloid		
	Corrosion Rate (mg/cm ² /h)	Surface Coverage	Inhib. Efficiency (%)	Corrosion Rate (mg/cm ² /h)	Surface Coverage	Inhib. Efficiency (%)
1 M HCl	0.934			0.934	-	-
300 ppm + 1 M HCl	0.457	0.51	51.1	0.310	0.67	66.8
500 ppm + 1 M HCl	0.296	0.68	68.3	0.162	0.83	82.6
750 ppm + 1 M HCl	0.205	0.78	78.1	0.095	0.90	89.8
1000 ppm + 1 M HCl	0.158	0.83	83.1	0.029	0.97	96.9
1250 ppm + 1 M HCl	0.110	0.88	88.2	0.022	0.98	97.7
1500 ppm + 1 M HCl	0.083	0.91	91.2	0.011	0.99	98.8

Hence,

$$C_{dl} = \frac{1}{2\pi f_{max} Z} \quad (6)$$

where f_{max} describe the maximum frequency of the semicircle and the π is 3.142.

However, the data for the IE_R % were obtained from the fitting of the charge transfer resistance values into Equation (7).

$$IE_R \% = \frac{R_{ct}^0 - R_{ct}^i}{R_{ct}^0} \times 100 \quad (7)$$

Figure 1(a–b) reveals a Nyquist plot with only one capacitive loop, and this may be due to the presence of just a single charge transfer (Go *et al.*, 2020; Wang, Chen, Han, Wang, & Hu, 2019a; He *et al.*, 2019; Ogunleye *et al.*, 2020). It was also observed that the size of the loops increased with the rise of both tubocurarine and aconitine alkaloid concentration up to 1500 ppm, which indicates that both inhibitors were adsorbed on the low carbon steel surface, and the surface area exposed to the 1 M HCl was reduced (Zaher *et al.*, 2020; Radwan, Sliem, Yusuf, Alnuaimi, & Abdullah, 2019; Shahzad *et al.*, 2020). This was analyzed in Table 2 as the charged transfer resistance values were seen increasing with increasing inhibitor concentration up to 1500 ppm. The double layer capacitance found decreases with increasing inhibitor concentration, and inhibition efficiency increases with the concentration increment. This proved strong adsorption of the inhibitor molecules on the metal surface (Go *et al.*, 2020; Solomon, Umoren, Quraishi, Tripathi, & Abai, 2020). It can also be said that the strong adsorption aid the system to overcome electron transfer from the positive electrode (anodic site) to the hydrogen ions in the solution hence blocking the corrosion reaction (He *et al.*, 2019; Tamalmani & Husin, 2020).

3.3 Potentiodynamic polarization

The corrosion rate is directly proportional to the corrosion current density (Shahzad *et al.*, 2020; Kwayyun & Msear, 2019). The plots and values obtained from the Potentiodynamic polarization experiment are presented in Table 5. Corrosion current density (I_{corr}) values were decreasing while inhibition efficiency ($\%IE_{I_{corr}}$) values were seen to increase with increasing inhibitor concentration, an indication that depicts decreasing diffusion rate for reactants to the surface of the metal and decreasing electrical resistance

Table 2. Electrochemical impedance data revealing charge transfer resistance of the metal, double layer capacitance, surface coverage, and inhibition efficiency of inhibitors on ASTM – A47 low carbon steel in 1 M HCl

	Inh. Conc.	R_{ct}	C_{dl}	θ	$\%IE$
	1 M HCl	122	1.3×10^{-5}	-	-
TBA	300 ppm	338	4.7×10^{-6}	0.639	63.9
	1000 ppm	683	2.3×10^{-6}	0.821	82.1
	1500 ppm	923	1.7×10^{-6}	0.868	86.8
ACA	300 ppm	268	5.9×10^{-6}	0.545	54.5
	1000 ppm	674	2.4×10^{-6}	0.819	81.9
	1500 ppm	770	2.1×10^{-6}	0.842	84.2

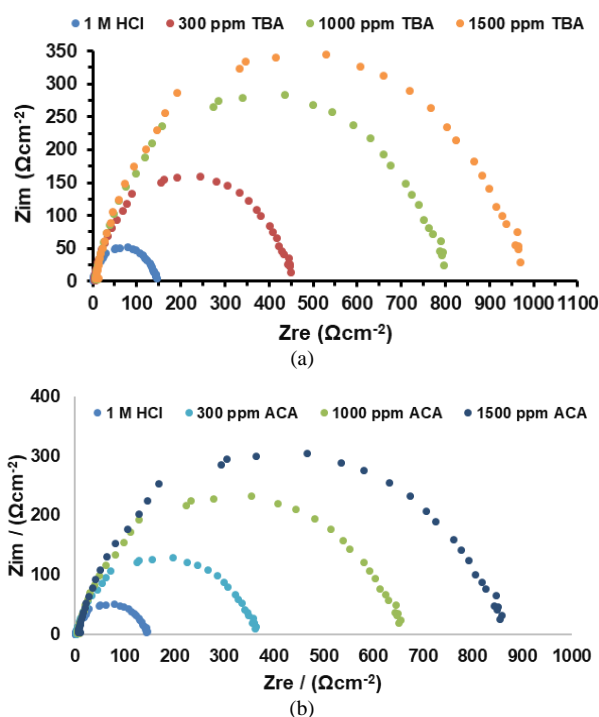


Figure 1. Nyquist plots for the corrosion inhibition of metal by (a) tubocurarine and (b) aconitine alkaloids on ASTM – A47 low carbon steel in 1 M HCl

of metal surface due to strength of bonding to the substrate, hence strong adsorption of inhibitor molecules (Solomon *et al.*, 2020). In addition, as shown in Figure 2 (a-b) and Table 3, the addition of tubocurarine and aconitine alkaloid molecules shifted the corrosion potential (E_{corr}) values away from the non-inhibited solution and also showed changes in both the cathodic and anodic polarization branches and values. These results indicate that the added inhibitors acted as mixed-type inhibitors (Tamalmani & Husin, 2020; Kwayyun & Msear, 2019).

3.4 Thermodynamics consideration

Figure 3 shows plots drawn from the temperature dependence data obtained from the gasometric methods. Values analyzed from the plots of $\ln CR$ against $1/T$, as shown in Table 4.

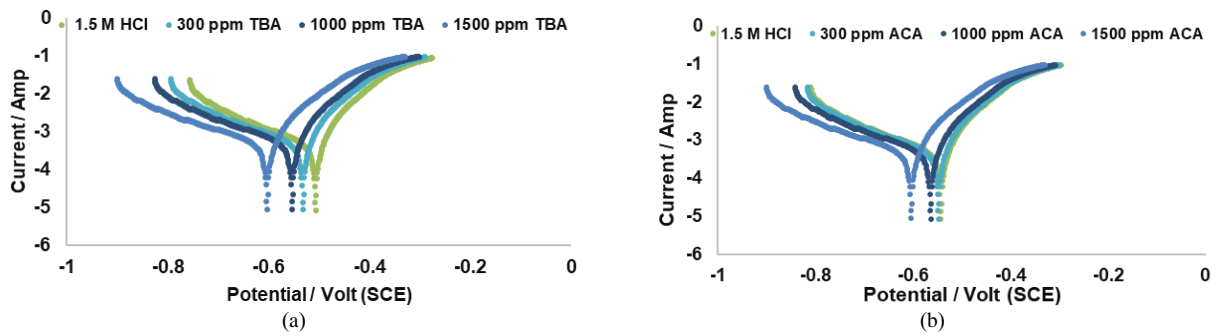


Figure 2. Tafel plots for ASTM – A47 low carbon steel corrosion in 1 M HCl acid solution with and without (a) tubocurarine and (b) aconitine alkaloids

Table 3. Potentiodynamic polarization data revealing corrosion current density, corrosion potential, Tafel slopes, and inhibition efficiency of inhibitors on ASTM – A47 low carbon steel in 1 M HCl

	Inh. Conc.	I_{corr} (mA cm ⁻²)	E_{corr} (mV)	β_c (mV/dec)	β_a (mV/dec)	θ	IE_i (%)
TBA	1 M HCl	2.106	-625	427	550	-	-
	300 ppm	0.847	-419	308	316	0.598	59.8
	1000 ppm	0.414	-295	274	173	0.803	80.3
	1500 ppm	0.269	-174	216	85	0.872	87.2
ACA	300 ppm	0.911	-743	357	319	0.567	56.7
	1000 ppm	0.524	-585	291	236	0.751	75.1
	1500 ppm	0.348	-321	200	170	0.835	83.5

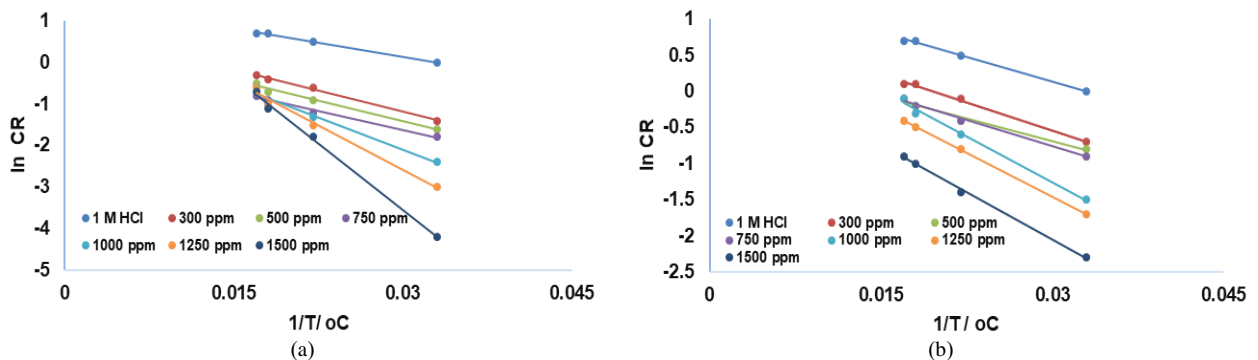


Figure 3. Arrhenius plots revealing the kinetics of corrosion reaction in the presence of (a) tubocurarine and (b) aconitine alkaloids inhibitors on ASTM – A47 low carbon steel in 1 M HCl

Table 4. Thermodynamic data revealing corrosion inhibition of (a) tubocurarine and (b) aconitine alkaloids on ASTM – A47 low carbon steel in 1 M HCl

	Inh. Conc.	A	E_a (kJ/mol)	ΔH (kJ/mol)	ΔS (kJ/mol)
Tubocurarine alkaloid	1 M HCl	1.5	3.74	28.267	49.72
	300 ppm	0.9	5.65	29.68	51.14
	500 ppm	0.5	5.39	24.27	45.73
	750 ppm	0.2	5.08	21.94	43.40
	1000 ppm	1.0	8.64	54.22	75.68
	1250 ppm	1.7	11.85	83.55	105.01
	1500 ppm	2.9	17.76	142.27	163.73
Aconitine alkaloid	300 ppm	1.0	4.29	28.40	49.86
	500 ppm	0.6	3.49	28.40	49.86
	750 ppm	0.7	4.02	82.56	104.02
	1000 ppm	1.3	6.99	34.86	56.32
	1250 ppm	1.0	6.71	29.69	51.15
	1500 ppm	0.6	7.23	50.87	72.33

$$CR = A \exp\left(\frac{-Ea}{RT}\right) \quad (8)$$

By taking the log of Equation 8, Equation 9 was obtained.

$$\ln CR = \ln A - \frac{Ea}{RT} \quad (9)$$

where k is the rate coefficient, A is the collision constant, R is the universal gas constant, T is the temperature (in kelvin), Ea is the amount of energy required to ensure that a reaction happens (Solomon *et al.*, 2020; Ugi, Bassey, Obeten, Adalikwu, & Nandi, 2020; Wang, Jiang, Zhang, Hou, & Zhou, 2019b). The collision coefficient or binding constant derived from Equation (11) was found to decreasing with inhibitor concentration but with a sudden increase from 1250 ppm to 1500 ppm concentration. This is an indication that the inhibitors, especially that of tubocurarine alkaloid, had a stronger binding tendency at higher concentrations. However, activation energy values were seen to be higher in the inhibited solution compared to the non-inhibiting solution (1 M HCl). This is apparently due to the strong adsorption of molecules of inhibitors onto the ASTM – A47 low carbon steel resized metals (Shahzad *et al.* 2020; Go *et al.*, 2020). This tendency can also be due to the physical adsorption mechanism of the inhibitor reaction. This has been seen as the activation energy values being less than 20 kJ/mol (Faiza *et al.*, 2020; Ugi *et al.*, 2020).

The Eyring transition state equation given in Equation (10) was adopted for the graphical determination of both the enthalpy and entropy of adsorption using the gasometric data that evolved from the experimental analysis.

$$\ln \frac{k}{T} = -\frac{\Delta H^\ddagger}{R} \frac{1}{T} + \ln \frac{kB}{h} + \frac{\Delta S^\ddagger}{R} \quad (10)$$

The values for ΔH^\ddagger and ΔS^\ddagger can be determined from kinetic data obtained from a plot of $\ln \frac{k}{T}$ vs. $\frac{1}{T}$. The straight line with a negative slope, $-\frac{\Delta H^\ddagger}{R}$, and a y-intercept, $\ln \frac{kB}{h} + \frac{\Delta S^\ddagger}{R}$ from the equation gives the two major thermodynamic parameters investigated. From Table 4 values of the enthalpy of adsorption were seen to be positive, an indication of endothermic reaction in the inhibitor-metal interface and possible absorption of energy (heat) by the inhibitor reacting system, leading to increase inhibitor reaction and limiting ionic transference at the anodic site of the metal

(Rajandran *et al.*, 2020; Majd *et al.*, 2020; Ugi *et al.*, 2020). This is in agreement with the inhibition efficiency result that shows decreasing efficiency while the temperature was increased. The values for the entropy of adsorption, as presented still in Table 4 show that the system was less disordered as values were negative. This situation will allow for the orderly and stable coverage of the inhibitors on the metal surface hence higher activation complex and advancement in the corrosion inhibition reaction (Tian & Zheng, 2019; Wang *et al.*, 2019a). The adsorption energy values are presented in Table 4. The values showed that the inhibitors presented negative free energy of adsorption, indicating that the inhibitors were stabled ones, and their reaction was spontaneous in the forward direction.

3.5 Adsorption evaluation

In an attempt to study the adsorption characteristics of the inhibitor molecules on the metal surface, the Langmuir, and El-Awady, adsorption isotherms were studied and constructed from Equation (11) and (12), respectively.

$$\frac{C}{q_e} = \frac{1}{k} + C \quad (11)$$

$$\log\left(\frac{\theta}{1-\theta}\right) = \log b + y \log C \quad (12)$$

where C is the concentration of inhibitors, q_e is the amount of adsorbate adsorbed per unit mass, k is the equilibrium constant, y is the number of inhibitor molecules occupying one active site, b is the heat of sorption, while the R and T take their usual meanings.

Generally, it was observed from Table 5 - 6 that the correlation coefficient values for the isotherms were approximately unity when fitted to the isotherms, and their isotherm equilibrium binding constants were decreasing with temperature. This implies that both isotherms were obeyed, and a physical adsorption process was eminent (Solomon *et al.*, 2020). The values of k for the Langmuir isotherm were found to be relatively large (> 1) for both inhibitors, an indication that there is a strong interaction between the inhibitors and the surface and a physical adsorption process (Ohtsuka *et al.*, 2018; Tamalmani & Husin, 2020). The El-Awady isotherm characterizes the adsorption sites on the metal surface. From the result in Table 6, values of 1/y are less than 1, confirming that both inhibitors occupied more than one active site, making them good inhibitors in 1 M HCl. (Ugi *et al.*, 2020).

Table 5. Langmuir data for the corrosion inhibition of (a) tubocurarine and (b) aconitine alkaloids on ASTM – A47 low carbon steel in 1 M HCl

Temp. (°C)	Aconitine alkaloid				Tubocurarine alkaloid			
	k	R	slope	ΔG (kJ/mol)	k	R	slope	ΔG (kJ/mol)
30	4.92	0.9713	0.7986	-13.99	1.55	0.9953	0.9272	-11.11
45	4.14	0.9943	0.9712	-13.56	1.22	0.9988	1.1141	-10.51
55	4.26	0.9899	1.016	-13.63	1.61	0.9987	1.1246	-11.21
60	6.42	0.9980	0.9399	-14.66	1.86	0.9986	1.1814	-11.57

Table 6. El-Awardy adsorption data for tubocurarine and aconitine alkaloids on ASTM – A47 low carbon steel in 1 M HCl

Temp. (°C)	Aconitine alkaloid				Tubocurarine alkaloid			
	1/y	R	y	ΔG (kJ/mol)	1/y	R	y	ΔG (kJ/mol)
30	0.01	0.9996	0.3	-14.69	0.16	0.9985	0.19	-5.45
45	0.2	0.9889	0.09	-9.01	0.13	0.9987	0.14	-7.39
55	0.19	0.9721	0.08	-10.77	0.19	0.9966	0.12	-10.77
60	0.14	0.9915	0.07	10.23	0.22	0.998	0.11	-12.48

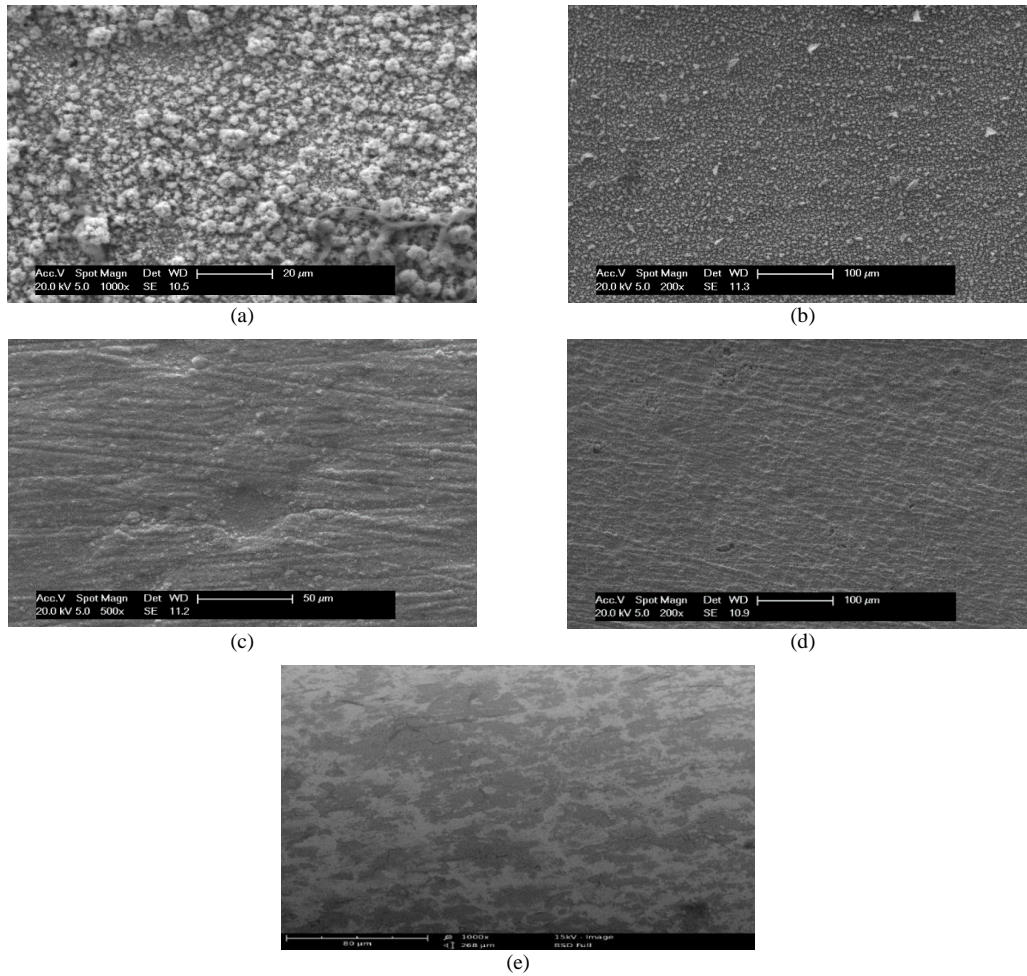


Figure 4. SEM micrographs of ASTM – A47 low carbon steel in (a) 1 M HCl, (b) 300 ppm ACA, (c) 300 ppm TBA, (d) 1500 ppm ACA and (e) 1500 ppm TBA

3.6 Surface morphology

Micrographs drawn from the scanning electron microscopic study are presented in Figure 4(a-e). A close observation on the slides shows a very rough surface for the metal immersed directly in the 1 M HCl solution. This is an indication of a direct acid attack on the surface, leading to the formation and possible evolution of hydrogen gas, giving rise to corrosion (Lavanya *et al.*, 2020; Radwan *et al.*, 2019). It was evident from the micrographs of metals immersed in inhibitor solution that the inhibitor molecules adsorbed strongly on the metal surface, hence blocking all anodic sites

from further corrosion as it were with those of the free solution (He *et al.*, 2019; Ugi *et al.*, 2020). However, the micrographs for the inhibition of metal by tubocurarine alkaloid at both inhibitor concentrations (300 ppm and 1500 ppm) presented better adsorption compared to those from aconitine alkaloid, and this confirmed the earlier assertions from other experimental results.

4. Conclusions

The research work presents the following findings. Tubocurarine and aconitine alkaloids inhibited at 98.9 and

91.2%, respectively, in the presence of 1 M HCl, indicating that they are good inhibitors of ASTM – A47 low carbon steel. Temperature dependence of the inhibitors revealed strong adsorption of inhibitors at lower temperatures, but however, inhibition was found increasing with the concentration of inhibitors at different temperatures. Thermodynamic data presented the inhibitors as stabled, spontaneous, physically adsorbed, and with a little or no degree of disorderliness. Electrochemical results revealed good adsorption performance by the inhibitors as charge transfer resistance was found increasing, double layer capacitance and polarization resistance were decreasing, and mixed-type inhibition was recorded. Adsorption consideration revealed that both inhibitors occupied more than one active site and as well as obeyed more of the Langmuir adsorption assumptions, hence monolayer. The surface morphology of the metals was smooth enough in both inhibitor concentrations hence strong bonding and large surface coverage.

References

- Al-Shehri, D. A. (2019). Oil and gas wells: Enhanced wellbore casing integrity management through corrosion rate prediction using an augmented intelligent approach, *Sustainability*, 11(3), 818.
- Bardal, E. (2004) *Corrosion and protection*. London, England: Springer-Verlag
- Bharatiya, U., Gal, P., Agrawal, A., Shah, M. & Sircar, A. (2019). Effect of corrosion on crude oil and natural gas pipeline with emphasis on prevention by ecofriendly corrosion inhibitors: A comprehensive review. *Journal of Bio- Tribo-Corrosion*, 5(2), 35.
- Davis, J. R. (2000). *Corrosion: Understanding the basics*. Geauga, OH: ASM International.
- Faiza, M., Zahari, A., Awang, K. & Hussin, H. (2020). Corrosion inhibition on mild steel in 1 M HCl solution by *Cryptocarya nigra* extracts and three of its constituents (alkaloids). *Royal Society of Chemistry Advances*, 10(11), 6547–6562.
- Gergely, A. (2019). *Phenomenal and theories in corrosion science: Methods of prevention*. Hauppauge, NY: Nova Science.
- Go, L. C., Depan, D., Holmes, W. E., Gallo, A., Knierim, K., Bertrand, T. & Hernandez, R. (2020) Kinetic and thermodynamic analyses of the corrosion inhibition of synthetic extracellular polymeric substances. *Peer Journal of Material Science*, 2, e4.
- He, T., Emori, W., Zhang, R. H., Okafor, P. C., Yang, M. & Cheng, C. R. (2019). Detailed characterization of *Phellodendron chinense* Schneid and its application in the corrosion inhibition of carbon steel in acidic media. *Bioelectrochemistry*, 130, 107332.
- Khayyun, T. S. & Mseer, A. H. (2019). Comparison of the experimental results with the Langmuir and Freundlich models for copper removal on limestone adsorbent, *Applied Water Science*, 9(8), 170.
- Lavanya, D. K., Priya, F. V. & Vijaya, D. P. (2020). Green approach to corrosion inhibition of mild steel in hydrochloric acid by 1-[morpholin-4-yl(thiophen-2-yl)methyl] thiourea. *Journal of Failure Analysis and Prevention*, 20(2), 494–502.
- Majd, M. T., Ramezanzadeh, M., Ramezanzadeh, B. & Bahlakeh, G. (2020). Production of an environmentally stable anti-corrosion film based on *Esfand* seed extract molecules-metal cations: Integrated experimental and computer modeling approaches. *Journal of Hazardous Material*, 382, 121029.
- McCafferty, E. (2010). *Introduction to corrosion science*. New York, NY: Springer-Verlag.
- Ogunleye, O. O., Arinkoola, A. O., Eletta, O. A., Agbede, O. O., Osho, Y. A., Morakinyo, A. F., & Hamed, J. O. (2020). Green corrosion inhibition and adsorption characteristics of *Luffa cylindrica* leaf extract on mild steel in hydrochloric acid environment. *Heliyon*, 6(1), e03205.
- Ohtsuka, T., Nishikata, A., Sakari, M., & Fushimi, K. (2018). *Electrochemistry for corrosion fundamentals*. Singapore: Springer.
- Radwan, A. B., Sliem, M. H., Yusuf, N. S., Alnuaimi, N. A. & Abdullah, A. M. (2019). Enhancing the corrosion resistance of reinforcing steel under aggressive operational conditions using behentrimonium chloride. *Science Report*, 9(1), 18115.
- Rajendran, S., Nguyen, T. A., Kakooei, S., Li, Y. & Yeganeh, M. (2020). *Corrosion Protection of the Nanoscale* (1st ed.). London, England: Elsevier.
- Roberge, P. R. (2008). *Corrosion engineering: Principle and practices*. Toronto, Canada: McGraw Hill Professional.
- Sangeetha, C., Chinnakani, C., Selvaraj, S. (2020). *Jatropha gossyfolia* – A green inhibitor act as anticorrosive agent on carbon steel. *Journal of Advance Science and Research*, 11(1), 180–186.
- Shahzad, K., Sliem, M., Shakoor, R. A., Radwan, A. B., Kahraman, R., Umer, M. A., . . . Abdullah, A. M. (2020). Electrochemical and thermodynamic study on the corrosion performance of API X120 steel in 3.5% NaCl solution. *Science Report*, 10(1), 4314.
- Solomon, M. M., Umoren, S. A., Qurashi, M. A., Tripathi, D. B. & Abai, E. J. (2020). Effect of alkyl chain length, flow, and temperature on the corrosion inhibition of carbon steel in a simulated acidizing environment by an imidazoline-based inhibitor. *Journal of Petroleum Science and Engineering*, 187, 106801.
- Talbot, D. E. J., & Talbot, J. D. R. (2018). *Corrosion science and technology* (3rd ed.). Boca Raton, FL: CRC Press.
- Tamalmani, K. & Husin, H. (2020). Review on corrosion inhibitors for oil and gas corrosion issues. *Applied Science*, 10(10), 3389.
- Tian, Y. & Zheng, M. (2019). Inhibition effect of silicate and molybdate on the corrosion of SS 316 in neutral corrosive solution at high temperature. *Material and Research Express*, 6, 096569.
- Ugi, B. U., Basse, V. M., Obeten, M. E., Adalikwu, S. A. & Nandi, D. O. (2020). Secondary plant metabolites of natural product origin-*Strongylodon macrobotrys* as pitting corrosion inhibitors of steel around heavy salt deposits in Gabu, Nigeria. *Journal of Material Science and Chemical Engineering*, 8(5), 38–60

- Wang, C., Chen, J., Han, J., Wang, C. & Hu, B. (2019a). Enhanced corrosion inhibition performance of novel modified polyaspartic acid on carbon steel in HCl solution. *Journal of Alloys and Compound*, 771, 736–746.
- Wang, X., Jiang, H., Zhang, D., Hou, L. & Zhou, W. (2019b) *Solanum lasiocarpum* extract as green corrosion inhibitor for A3 steel in 1 M HCl solution. *International Journal of Electrochemical Science*, 14, 1178–1196.
- Zaher, A., Chaouiki, A., Salghi, R., Boukhraz, A., Bourkhiss, B. & Ouhssine, M. (2020). Inhibition of mild steel corrosion in 1M hydrochloric medium by the methanolic extract of *Ammi visnaga* L. Lam seeds, *International Journal of Corrosion*, 2020, 9764206